

Visualization of enantio recognition by excited-state conformation modulation

Received: 6 May 2025

Accepted: 8 August 2025

Published online: 21 August 2025

Zizhao Huang^{1,2}, Ying Hu^{1,2}, Jie Sun¹, Zhenyi He¹, Tao Jiang¹ , He Tian¹ & Xiang Ma¹ ✉

Chiral purity is crucial in life sciences, emphasizing the importance of precise enantiomeric identification and the development of analytical techniques. Here, we design functional dyes with visual chiral recognition capabilities by introducing recognition units 2-amino-1,2-diphenylethanol into vibration-induced emission molecules. The unambiguous differentiation in luminescent colors upon binding to enantiomers facilitates the efficient recognition of enantiomers and the analysis of enantiomeric excess. The chiral recognition process originates from co-assembly under charge-aided hydrogen bonding interactions, which is significantly impacted by the steric hindrance effect, and further affects the planarization of the excited state conformation of the dye. This co-assembly process precisely amplifies the dynamics at the molecular level into macroscopic observable signals for real-time, highly sensitive recognition. Furthermore, we establish a sophisticated optical analysis system by correlating Red-Green-Blue values and CIE coordinates to analyze the enantiomeric excess of chiral molecules. This work opens a distinct avenue for visual chiral recognition and inspires the development of advanced optical materials in chiral sensing chemistry.

Chirality, a fundamental aspect of molecular structure, plays a pivotal role in various fields ranging from pharmaceuticals to materials science; therefore, the ability to discern and separate enantiomers is of paramount importance^{1–5}. Luminescence-based techniques have emerged as a compelling alternative to High-performance liquid chromatography, offering the advantages of simplicity, high speed and the potential for real-time monitoring^{6–11}. Nevertheless, the sensitivity of macroscopic measurements in chiral recognition processes is often diminished due to the influence of ensemble averaging effects. Although scientists have achieved numerous research outcomes in the field of developing chiral recognition technologies using functional dyes^{12–15}, there remains an urgent demand for facile, rapid and sensitive chiral recognition products. The pivotal and challenging lie in exploiting the differential interactions between the dye and the enantiomers to precisely modulate the emission energy levels of dyes, thereby enabling high-sensitivity discrimination between enantiomers^{16–18}.

A recent study from Tian's group indicated that a class of fluorophore exhibited the vibration-induced emission (VIE) effect^{19–21}. The molecules in solution undergo an excited-state configuration transformation, inducing the effective p-conjugation thus emitting red fluorescence. While in the solid or aggregation state, the physical constraint blocked the planarization of the structure in the excited state, result in an emission of intrinsic blue light. Unlike traditional fluorophores, VIE dyes exhibit fluorescence that is dynamically modulated by changes in their microenvironment^{22,23}. This sensitivity of the excited state allows for the amplification of subtle variations in assembly within the chiral space, rendering VIE dyes particularly suitable for chiral discrimination. Guo et al²⁴ utilized VIE with graphene to construct a single-molecule device, enabling in situ and real-time direct observation of chirality recognition at the single-molecule level through the discrimination of electrical conductance states. However, sample pretreatment before instrumental detection and following

¹Key Laboratory for Advanced Materials and Feringa Nobel Prize Scientist Joint Research Center, Frontiers Science Center for Materiobiology and Dynamic Chemistry, School of Chemistry and Molecular Engineering, East China University of Science and Technology, Shanghai, China. ²These authors contributed equally: Zizhao Huang, Ying Hu. ✉e-mail: maxiang@ecust.edu.cn

analysis were carried out under harsh conditions. Here, we were committed to accurately amplify the microscale dynamic variations at the single-molecule level to a macroscopic state that is perceptible to the unaided eye, thereby facilitating real-time, highly sensitive, and visual chirality discrimination.

Hence, we designed and synthesized functional materials with visual chiral recognition capabilities by introducing recognition units 2-Amino-1,2-Diphenylethanol into VIE molecules. As shown in Fig. 1, by utilizing the selective co-assembly mechanism between the dyes and chiral small molecules, we precisely modulated the excited-state conformation of VIE dyes under assembly conditions. The differentiation in luminescent color enabled the recognition of enantiomers and the analysis of enantiomeric excess. Additionally, by employing digital photography and handheld optical detector for the quantification Red-Green-Blue (RGB) values and CIE coordinates with the enantiomeric excess, thereby establishing an optical display system for analyzing the enantiomeric excess of chiral small molecules.

Results

Preparation and characterization of the chiral recognition dyes

The chiral color indicator was obtained by introducing chiral recognition auxiliary (1*S*,2*R*)- or (1*R*,2*S*)-1,2-diphenyl-2-aminoethanol into VIE dyes with an alkyl chain as a bridging unit (see Supplementary Fig. 1 for details of the chemical structure). ¹H NMR, ¹³C NMR, and electronic spray ionization (ESI) high-solution mass spectroscopy analyses were employed to confirm their structures (detailed characterization data see Supplementary Figs. 25–34).

The 1,2-diphenyl-2-aminoethanol moiety serves as the impetus for chiral recognition, attributable to its enantiomer-specific “oriented attachment” interactions with chiral molecules. The precise orientation and spatial arrangement enable it to form specific non-covalent interactions^{25–27}. As shown in the fluorescence spectra, (1*S*,2*R*)-DPAC exhibited typical vibration-induced emission properties, which presented different emissive behaviors in solid state and solution, indicating that the introduction of the chiral recognition auxiliary will not affect the transformation on the excited-state configuration of the VIE dye (Fig. 2a, b and Supplementary Fig. 2).

Visualization of enantiorecognition

Subsequently, we undertook an analytical assessment to quantify the stereoselective binding affinity of (1*S*,2*R*)-DPAC for enantiomeric analytes. As shown in fluorescence spectra (Fig. 2c), the fluorescence curve of the freshly prepared (1*S*,2*R*)-DPAC solution showed a strong

red emission at 600 nm. The addition of (1*R*,2*R*)-cyclohexane-1,2-dicarboxylic acid (*R*-1) resulted in a significant decrease in fluorescence intensity at 600 nm, along with the appearance of a emission band at 460 nm. The sample exhibited a perceptible color transformation from an initial red to a distinct blue, and after the addition of 2.0 equivalents of *R*-1, results in no discernible alteration in photoluminescence. Comparatively, upon the incorporation of a chiral compound with an alternative stereoisomeric conformation (1*S*,2*S*)-cyclohexane-1,2-dicarboxylic acid (*S*-1), the resultant luminescent perturbation within the system was observed to be markedly attenuated (Fig. 2d). Due to the dual emission characteristics of the VIE, the ratiometric fluorescence ($I_{460\text{ nm}}/I_{600\text{ nm}}$) exhibited significant variation in response to the titration of chiral compounds with different conformations. Additionally, we consequently investigated the optimal concentration and solvent ratio to maximize the visual discrimination capability (Supplementary Figs. 3 and 4). Hence, examination of the photo and the CIE coordinated diagram revealed that the luminescent properties exhibited pronounced differences when various enantiomers were introduced under optimal conditions (Fig. 2e, f). And the high quantum yield of this process facilitated the visual discrimination of chirality without the necessity for laborious multistep operation (Supplementary Fig. 5). This streamlined approach significantly enhanced the efficiency and applicability of chiral detection (Supplementary Movie 1).

Based on the above-mentioned phenomenon, we investigated other common aromatic chiral compounds and amino acids, (1*S*,2*R*)-DPAC consistently demonstrated exceptional capability in visual chiral discrimination. Upon the addition of 2.0 equivalents of chiral compounds with different conformations, either of them exhibited a distinct luminescent disparity in cyclohexane/acetone (5/1, v/v) (Supplementary Figs. 6–9). Leveraging this property, we achieved the quick recognition of the chiral compound configurations by simple visible inspection. This encompasses amino acids and their derivatives, chiral acids, as well as pharmaceuticals such as mandelic acid, among others, which demonstrate a broad generalizability (Table 1 and Supplementary Figs. 10–12). Given the distinctive nature of structure 1,2-diphenyl-2-aminoethanol, which possesses two chiral centers, it is not predestined to manifest a heightened binding affinity exclusively for the *R*-enantiomer. Conversely, there are scenarios wherein a more pronounced affinity is observed with the *S*-enantiomer. Nonetheless, the variable binding affinities associated with different conformational molecules invariably facilitate the enantioselective recognition capability.

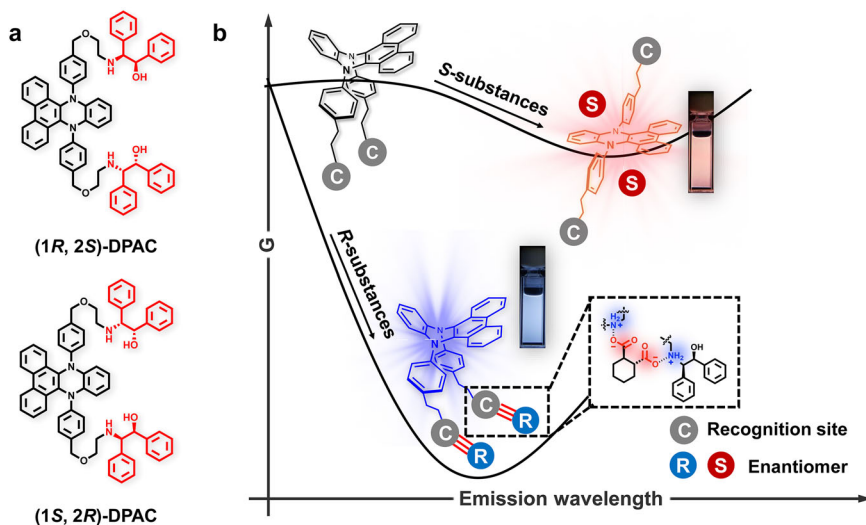


Fig. 1 | Structure and characterization of the enantiorecognition. **a** Structures of chiral molecules (1*S*,2*R*)- and (1*R*,2*S*)-DPAC. **b** Schematic representation of the visualization of enantiorecognition.

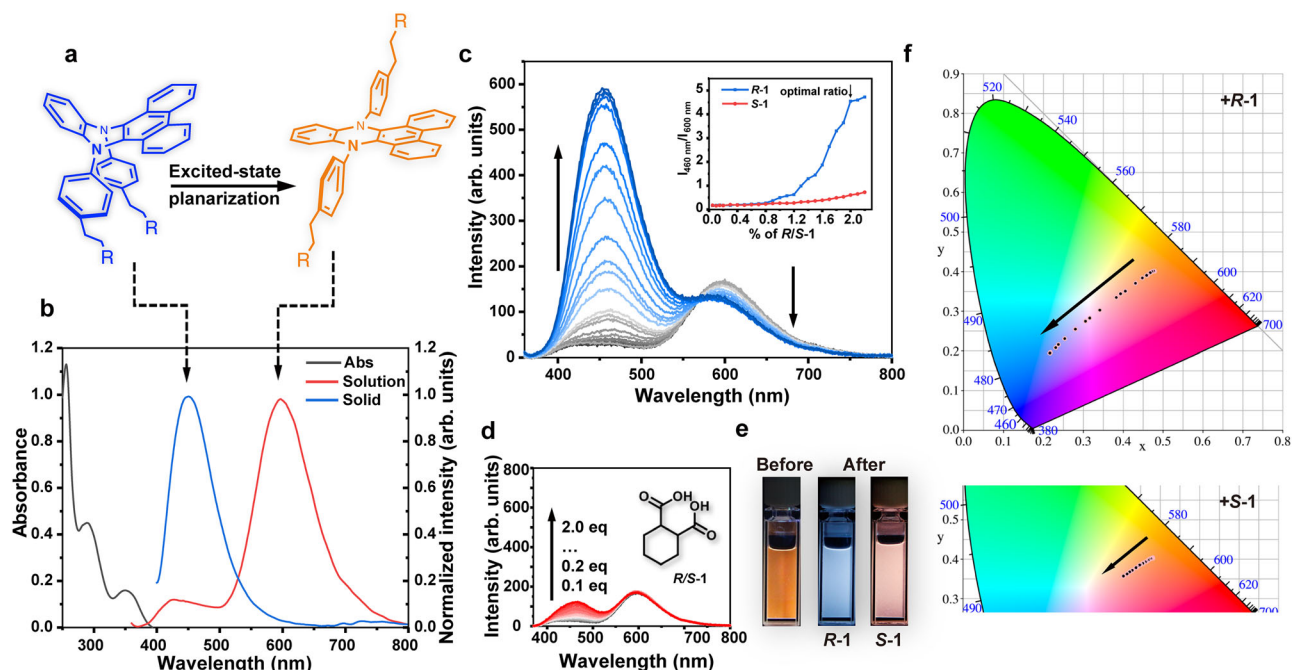


Fig. 2 | Optical characteristics of enantirecognition. **a** Schematic illustration of the VIE mechanism. **b** The absorbance and fluorescence spectra of (1S,2R)-DPAC, [(1S,2R)-DPAC] = 1.0×10^{-5} M in acetone, $\lambda_{\text{ex}} = 350$ nm. The fluorescence spectra of (1S,2R)-DPAC after being mixed with **c** R-1 and **d** S-1 in different ratios (0.00–2.00

equiv), Inset: the ratiometric fluorescence intensity. **e** The photo of (1S,2R)-DPAC before and after being mixed with R/S-1. **f** The corresponding 1931 CIE coordinated diagram of (1S,2R)-DPAC after being mixed with R/S-1 in different ratios. [(1S,2R)-DPAC] = 1.0×10^{-4} M in cyclohexane/acetone 5:1, $\lambda_{\text{ex}} = 350$ nm.

Mechanisms of visualization recognition

Drawing upon the principles of VIE, the observed pronounced variations in photoluminescent emission may be ascribed to the formation of diverse molecular aggregational states. Within these structurally rigidified assemblies, the process of excited-state planarization induced by vibration was markedly attenuated, which in turn engenders the emission of intrinsic blue fluorescence. Hence, from the perspective of morphology characterization to confirm our hypothesis, the self-assembly process was investigated by dynamic light scattering (DLS). In this particular mixed solvent system, the introduction of chiral molecules into a (1S,2R)-DPAC system resulted in a discernible alteration in the particle size of the dye, thereby substantiating the formation of diverse assemblies (Fig. 3a). In the absorption spectra, the scattering effects that arise from the formation of aggregates were also be clearly observed (Supplementary Fig. 13). Besides, the rigidification effect of the assembly efficiently suppressed the non-radiative transition of fluorescence, resulting in a significant enhancement of the luminescence lifetimes at both 460 nm and 600 nm (Fig. 3c).

The principal determinant of enantioselectivity is predominantly the enthalpic variations, with the phenomenon of enthalpy-entropy compensation likewise identified as a significant factor in modulating enantioselectivity^{28–30}. The amino group within the molecular structure of (1S,2R)-DPAC was recognized as an efficacious proton receptor, which was predisposed to engage in the formation of ionic complexes in an acidic milieu. We speculate that the solubility of the formed ionic compound will decrease, which was a pivotal factor in the formation of aggregates and the alteration of the excited-state conformation of VIE molecules. Subsequently, we employed an inorganic acid (hydrochloric acid) to facilitate the precipitation of ionic compounds via titration methodology. As illustrated in the Fig. 3b, with the increment of hydrochloric acid at various molar ratios, (1S,2R)-DPAC manifested an analogous trend in luminescence variation. Furthermore, two reference compounds were chosen for this investigation: R-Dic, which is devoid of proton-donating capability, and D-Glu, characterized by its enhanced basicity. The results indicated that neither of these

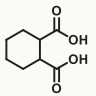
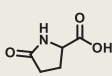
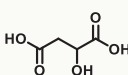
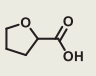
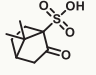
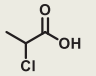
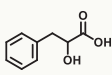
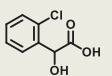
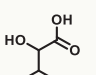

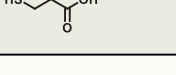
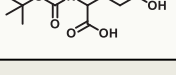
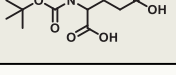
compounds could induce the formation of the ($-\text{NH}_2^+$) structure in (1S,2R)-DPAC, consequently failing to cause a change in luminescent color (Fig. 3d). Therefore, the assembly of (1S,2R)-DPAC with chiral acid molecules were orchestrated through charge-aided hydrogen bonding interactions, which acted as the impetus for the modulation of photoluminescent properties.

In pursuit of a profound elucidation of the operational mechanisms governing the enantioselective recognition process, ^1H NMR titration was utilized to delineate the specific binding sites where the (1S,2R)-DPAC engaged with chiral molecular entities. However, due to the precipitation of molecular aggregates resulting from solubility diminished upon the mixed (1S,2R)-DPAC with R-1 in $(\text{CD}_3)_2\text{CO}$, which impedes the detection of intermolecular interaction signals in ^1H NMR, we opted to utilize CDCl_3 as a solvent medium. As illustrated in the provided Fig. 3e, the assembly of (1S,2R)-DPAC with R-1 results in a significant perturbation of the proton resonances for both constituents. The acquired amino group ($-\text{NH}_2^+$) exhibits a significant capacity to diminish the electron density surrounding adjacent protons, thereby inducing a pronounced downfield displacement in the NMR spectral profile. These results conclusively demonstrate that the formation of $-\text{NH}_2^+$ are pivotal for the altered luminescence and the basis for visual chiral characterization.

Enantioselective interaction

Circularly polarized luminescence (CPL) reflects the excited-state structural information of chiral luminescent systems^{31–33}. Upon the addition of enantiomers, the CPL of (1S,2R)-DPAC exhibited a trend consistent well with its fluorescence spectra. The constancy in the direction of the circular dichroism (CD) and CPL spectrum suggested that the interaction with chiral small molecules does not induce any modification to the chiroptical configuration of (1S,2R)-DPAC (Fig. 4a, Supplementary Figs. 15–18). Accordingly, upon unequivocally establishing the non-occurrence of configurational inversion, we performed geometric optimization based on the B3LYP/6-311g* model to determine of the atomic configuration of a molecule in its lowest energy

Table 1 | The fluorescence intensity ratio and CIE of the mixture of the two enantiomers with (1*S*,2*R*)-DPAC

No	Chemical Structure	$I_{\text{ratio}}/I_{\text{ratio}}$	CIE (R/S or D/L)
1		7.59 (RR/SS)	(0.21,0.19)/(0.39,0.34)
2		1.91 (R/S)	(0.28,0.28)/(0.34,0.34)
3		2.32 (R/S)	(0.22,0.19)/(0.30,0.26)
4		2.08 (R/S)	(0.33,0.29)/(0.40,0.34)
5		1.85 (R/S)	(0.21,0.21)/(0.26,0.25)
6		1.58 (R/S)	(0.29,0.25)/(0.34,0.29)
7		5.00 (R/S)	(0.25,0.24)/(0.40,0.35)
8		2.39 (S/R)	(0.28,0.25)/(0.21,0.21)
9		2.72 (R/S)	(0.22,0.21)/(0.31,0.28)
10		2.17 (D/L)	(0.30,0.27)/(0.37,0.33)
11		2.07 (D/L)	(0.29,0.27)/(0.23,0.21)
12		2.22 (D/L)	(0.26,0.25)/(0.34,0.28)
13		5.54 (L/D)	(0.31,0.28)/(0.19,0.17)

All the measurement under the condition of [(1*S*,2*R*)-DPAC] = 1×10^{-4} M in cyclohexane/acetone 5:1, [(1*S*,2*R*)-DPAC]/[enantiomers] = 1/2.

I_{ratio} represents the ratiometric fluorescence of $I_{460 \text{ nm}}/I_{600 \text{ nm}}$.

state. The calculated energies of (1*S*,2*R*)-DPAC after being mixed with *R/S*-1 indicate that they prefers to stack in a U-pattern with lower potential energy (Fig. 4c). Based on this optimal structure, we employed the M06-2X/DEF2-TZVP suite to calculate the interaction energies between (1*S*,2*R*)-DPAC and the enantiomers of *R/S*-1. After the

counterpoise correction, the interaction energies of (1*S*,2*R*)-DPAC with the *R* and *S* enantiomers were determined to be -22.49 kcal/mol and -19.49 kcal/mol, respectively. Additionally, the binding behavior between (1*S*,2*R*)-DPAC and *R/S*-1 was estimated by isothermal titration calorimetry (ITC) experiments. The ITC data unambiguously reveal the disparities in binding constants among enantiomers (Fig. 4b and Supplementary Fig. 19).

Furthermore, disparities in the interactions were also found through morphological characterization. The interaction of (1*S*,2*R*)-DPAC with *R/S*-1 of distinct conformations engenders a pronounced disparity in particle number. Specifically, the assembly was formed subsequent to the interaction with *R*-1 compounds and exhibited an augmented particle size and a concomitant increase in quantity (Supplementary Figs. 20, 21). Hence, upon the encounter of an enantiomer of an acid with an appropriate stereochemical configuration that is compatible with (1*S*,2*R*)-DPAC, an aggregate was formed resulting from solubility diminished. This aggregation inhibits the planarization of the excited state of (1*S*,2*R*)-DPAC induced by vibration, culminating in the emission of blue light (Fig. 4d). Therefore, any condition parameters that can modulate the solubility of the aggregates will concomitantly impact the alterations in emission characteristics (Supplementary Fig. 3 and 4).

Enantiomeric excess analysis

The enantiomeric acids' stereoselective assembly with (1*S*,2*R*)-DPAC endows the supramolecular complex with tunable luminescent properties. The luminescence distinctions arising from these wavelength variations will render the differentiation between enantiomers more pronounced, which hold promise for the development of analytical techniques with high fidelity and sensitivity for the quantification of enantiomeric excess (ee%) in chiral small molecules. We considered the exemplar case of the *R/S*-1. Upon maintaining the molar ratio of (1*S*,2*R*)-DPAC to the chiral molecule at 1:2, a systematic attenuation of the ratiometric fluorescence ($I_{460 \text{ nm}}/I_{600 \text{ nm}}$) intensity of (1*S*,2*R*)-DPAC was observed in correlation with the enantiomeric excess, spanning the complete spectrum from +100% to -100% (Fig. 5a). Conversely, (1*R*,2*S*)-DPAC manifests a near-perfect mirror symmetry. A pronounced nonlinear relationship exists between the ratiometric fluorescence intensity and the enantiomeric excess. Consequently, by fitting the curve, it served as a calibration curve for determining the enantiomeric composition of unknown ee % values. This allowed quantitative determination of the ee% from the fluorescence spectral changes. Furthermore, the establishment of a relationship between ratiometric fluorescence intensity and ee% allowed for the circumvention of the influence of testing conditions on the detection signal. Hence, we determined several sets of unknown samples under various testing conditions, yielding an average absolute error (AAE) between the measured and actual ee values of 2.55% (Supplementary Fig. 22 and Supplementary Table 1).

The establishment of optical analytical system

Distinct variations in the luminescent color under different ee% were readily discernible from both the CIE diagram and the images (Fig. 5b). Such pronounced alterations in luminescent color allowing approximate determination of the ee% values by visual inspection, offer a constructive strategy for the development of a visualizable ee% colorimetric sensor. Henceforth, we procured photographic documentation of luminescent emissions across a spectrum of ee% values. Nevertheless, acknowledging the inherent variability in the photosensitive components among disparate imaging apparatuses and the potential for environmental luminance to exert influence over the photographic outcome, we implemented a standard color reference card to correct for the veracity of the luminescent conditions exhibited by the specimens (Supplementary Figs. 23 and 24). Hence, employing digital photographic techniques, the unknown specimens

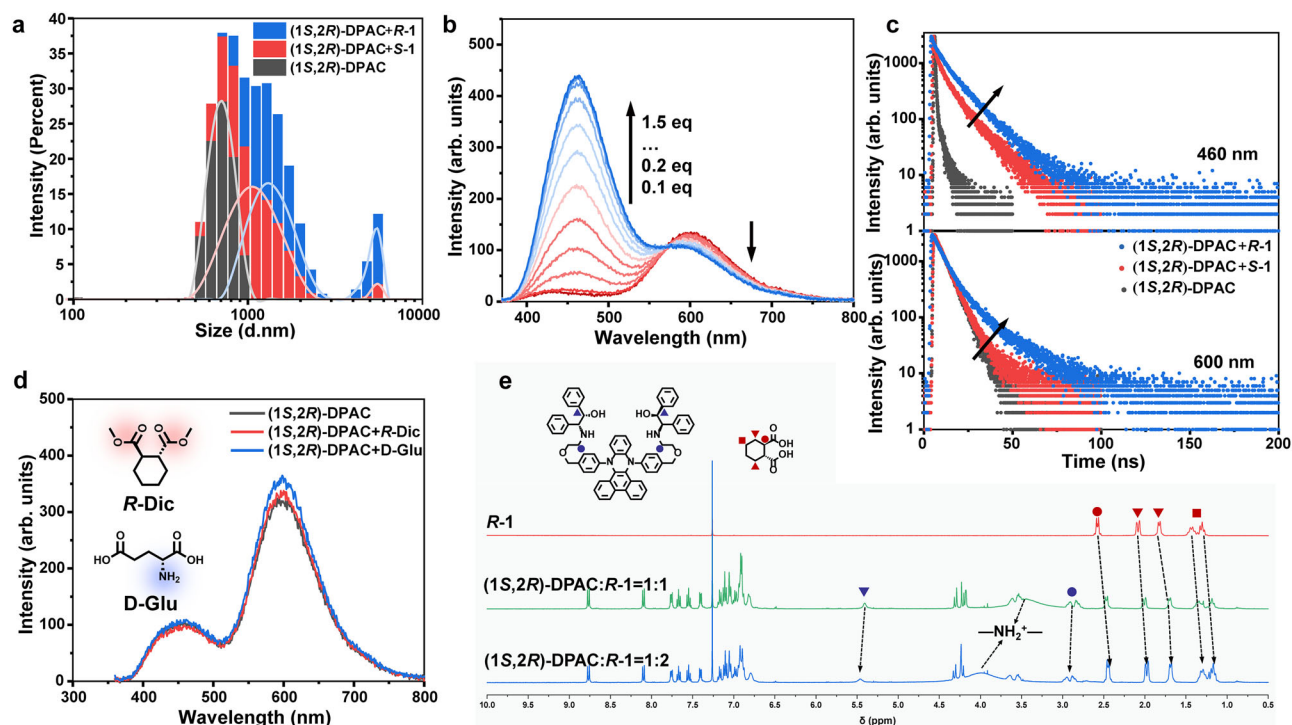


Fig. 3 | Mechanisms of visualization recognition. **a** The DLS of (1S,2R)-DPAC after being mixed with R/S-1. **b** The fluorescence spectra of (1S,2R)-DPAC after being mixed with HCl in different ratios. **c** The luminescent decay lifetimes of (1S,2R)-DPAC after being mixed with R/S-1. **d** The fluorescence spectra of (1S,2R)-DPAC

after being mixed with R-Dic and D-Glu. [(1S,2R)-DPAC] = 1.0×10^{-4} M in cyclohexane/acetone 5:1, [(1S,2R)-DPAC]/[enantiomers] = 1/2, λ_{ex} = 350 nm. **e** ¹H NMR spectra (400 MHz, 298 K) of (1S,2R)-DPAC after being mixed with R-1 in CDCl₃.

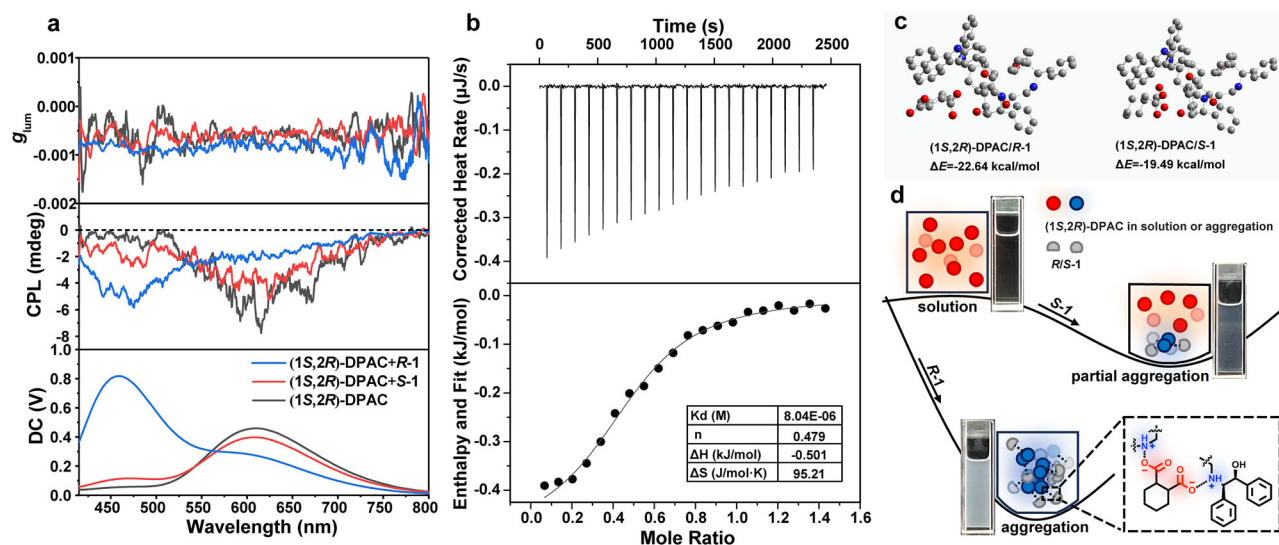


Fig. 4 | Enantioselective interaction and geometric optimization. **a** The CPL of (1S,2R)-DPAC after being mixed with R/S-1. [(1S,2R)-DPAC] = 1.0×10^{-4} M in cyclohexane/acetone 5:1, [(1S,2R)-DPAC]/[enantiomers] = 1/2, λ_{ex} = 350 nm. **b** ITC data for (1S,2R)-DPAC with R-1 in acetone. [(1S,2R)-DPAC] (cell) = 100 μM, [R-1]

(syringe) = 1 mM, 298 K. **c** The structures and interaction energies between (1S,2R)-DPAC and the enantiomers of R/S-1 based on the B3LYP/6-311 g* level and M06-2X/DEF2-TZVP suite. **d** Schematic representation of the visualization of enantiorecognition.

were rendered into their respective red, green and blue values (Fig. 5c and d). However, the variation in RGB values exhibits a linear relationship only at specific values of ee%, which may slightly affect practical applications.

Subsequently, we employed a handheld optical testing instrument capable of directly acquiring optical data from the samples, such as CIE coordinates. Consequently, we plotted the relationship between CIE coordinates and the ee%, which demonstrated a

significant linear correlation. This approach substantially enhanced the sensitivity and convenience of the detection process (Fig. 5d and supplementary Table 2). Thereby, it is possible to deduce the ee % of said samples through an analysis of the luminance profiles across the RGB channels or CIE coordinates without using any spectroscopic instruments (Fig. 5e). The simplicity of this strategy demonstrates significant potential in the identification of chiral reagents.

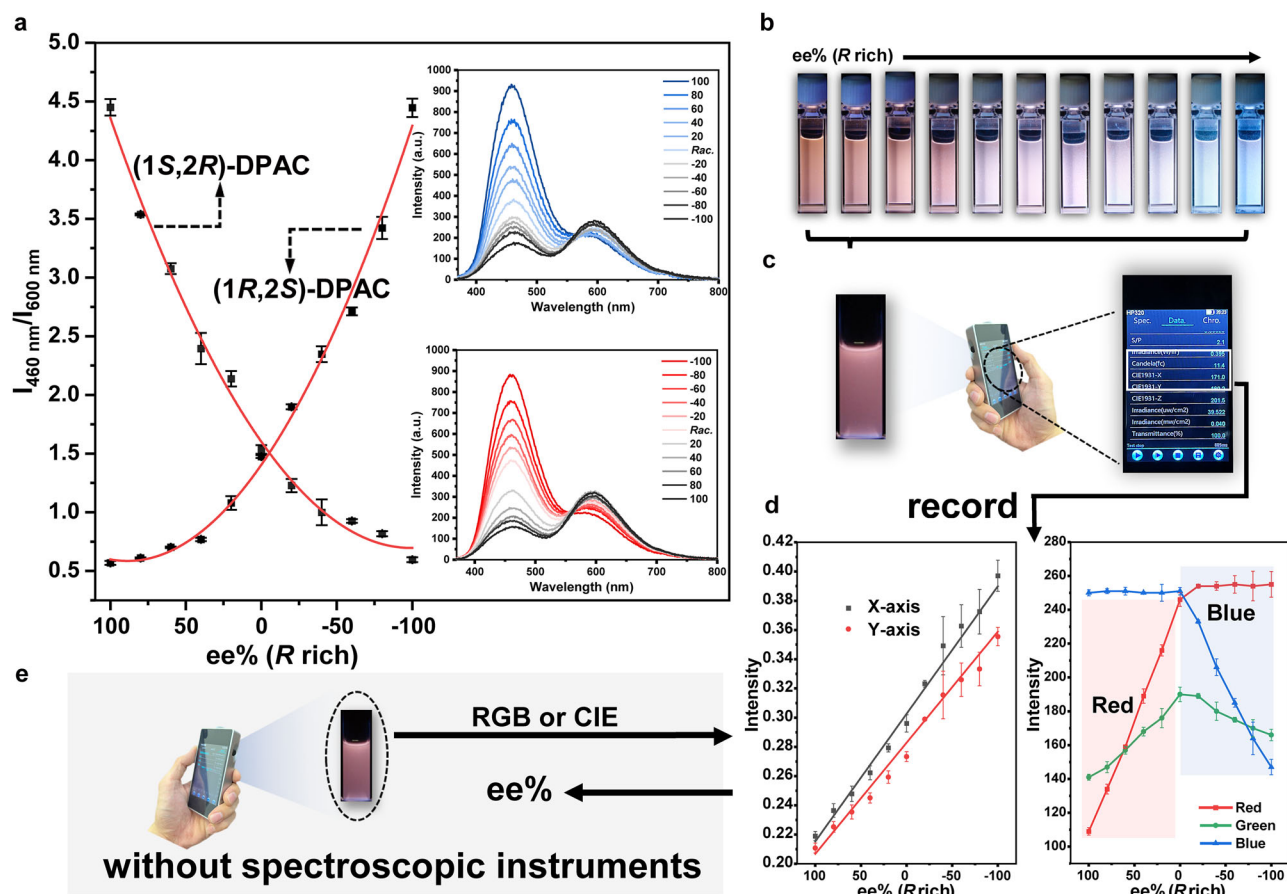


Fig. 5 | Optical characteristics of enantiomeric excess analysis. **a** Change of relative fluorescence intensity ratios of 460 nm/600 nm of (1S,2R)- or (1R,2S)-DPAC after being mixed with various enantiomer content of R/S-1. Inset: the fluorescence spectra of (1S,2R)- or (1R,2S)-DPAC after being mixed with various enantiomer content of R/S-1. **b** The photo of (1S,2R)-DPAC after being mixed with various enantiomer content of R/S-1. **c** The schematic cartoon illustration of the

recording CIE coordinates by handheld optical testing instrument. **d** Plots of the CIE coordinates and RGB values versus $ee\%$ of R/S-1. (Data with error bars are expressed as mean \pm s.d., $n = 3$ independent samples). **e** The schematic cartoon illustration of the enantiomer excess analysis. [(1S,2R)- or (1R,2S)-DPAC] = 1.0×10^{-4} M in cyclohexane/acetone 5:1, [(1S,2R)- or (1R,2S)-DPAC]/[R/S-1] = 1/2, $\lambda_{\text{ex}} = 350$ nm.

Discussion

In conclusion, a functional probe with visual chiral recognition capabilities by introducing recognition units 2-amino-1,2-diphenylethanol into vibration induced emission molecules was designed and synthesized. By leveraging non-covalent interactions to drive the selective assembly between dyes and chiral small molecules, we meticulously modulated the excited-state conformation of VIE dyes. This precise manipulation enabled the visual discrimination of various chiral compounds. Besides, the differentiation in luminescent colors enabled the recognition of enantiomers and the analysis of enantiomeric excess. Further, into RGB values and CIE coordinates and subsequent quantification, an optical display system was established for the analysis of enantiomeric excess in chiral small molecules. This strategy provides a facile and convenient method for enantioselective recognition and the analysis of enantiomeric excess.

Method

Materials

All solvents employed were commercially available and used as received without further purification. All enantiomers were commercially available and used as received without further purification (Purity >98%). The molecular structures were confirmed using ^1H NMR, ^{13}C NMR, and high-resolution ESI mass spectroscopy or MALDI-TOF mass spectroscopy.

General methods

^1H NMR and ^{13}C NMR spectra were measured on a Bruker AV-400 and Ascend 600 spectrometer. The ESI high-resolution mass spectra were tested on a Waters LCT Premier XE spectrometer. The UV-Vis absorption spectra and PL spectra were performed on a Varian Cray 500 spectrophotometer and a Varian Cary Eclipse spectrophotometer at 25 $^{\circ}\text{C}$, respectively. Quantum yields were measured by using an integrating sphere on a HAMAMATSU Quantaurus-QY C11347-11. DLS was carried out on a MALVERN, ZETA SIZER, model ZEN3600, 25 $^{\circ}\text{C}$. CPL spectra were acquired using the JASCO CPL-200 spectrofluoropolarimeter. CD spectra were acquired using the JASCO J815 spectrophotometer. Fluorescence lifetimes were measured on Edinburgh Instruments Fluorescence Spectrometer (FLS1000). No special instructions, the photos were taken by Canon 60D, UV irradiation source was used from tunable 365 nm LED lamp with 16.7 mW/cm 2 . The handheld optical testing instrument was used from Hangzhou LCE Intelligent Detection Instrument Co., Ltd. HP 320. SEM images were obtained by using a S-3400N (droplets of the sample solution (1×10^{-5} M) were applied to a silicon slice and dried in air at room temperature, and then coated with nano Au in a vacuum).

Geometric optimization

The structures and interaction energies between (1S,2R)-DPAC and the enantiomers of R/S-1 based on the B3LYP/6-311 g* method and M06-2X/DEF2-TZVP method.

Data availability

All relevant data that support the findings are available within this article and supplementary information and are also available from corresponding authors upon request. Source data are available. Source data are provided with this paper.

References

- Sripada, A., Thanzeel, F. Y. & Wolf, C. Unified sensing of the concentration and enantiomeric composition of chiral compounds with an achiral probe. *Chem* **8**, 1734–1749 (2022).
- Huang, J. H. et al. Carborane-cluster-wrapped copper cluster with cyclodextrin-like cavities for chiral recognition. *J. Am. Chem. Soc.* **146**, 16729–16736 (2024).
- Yuan, C. et al. Are highly stable covalent organic frameworks the key to universal chiral stationary phases for liquid and gas chromatographic separations. *J. Am. Chem. Soc.* **144**, 891–900 (2022).
- Sun, G. et al. Chiral macrocycles for enantioselective recognition. *J. Am. Chem. Soc.* **146**, 26233–26242 (2024).
- Vogwell, J., Rego, L., Smirnova, O. & Ayuso, D. Ultrafast control over chiral sum-frequency generation. *Sci. Adv.* **9**, ead1429 (2023).
- Kubo, Y., Maeda, S. Y., Tokita, S. & Kubo, M. Colorimetric chiral recognition by a molecular sensor. *Nature* **382**, 522–524 (1996).
- Wang, S. et al. Self-reporting activated ester-amine reaction for enantioselective multi-channel visual detection of chiral amines. *Angew. Chem. Int. Ed.* **61**, e202202268 (2022).
- Pu, L. Enantioselective fluorescent recognition of free amino acids: challenges and opportunities. *Angew. Chem. Int. Ed.* **59**, 21814–21828 (2020).
- Wang, X. et al. Visualization of enantioselective recognition and resolution by chiral AIEgens. *ACS Nano* **16**, 8223–8232 (2022).
- Qi, C. et al. Visualization of enantioselective recognition and separation of chiral acids by aggregation-induced emission chiral diamine. *Aggregate* **4**, e299 (2022).
- Oehler, S. et al. A DNA-encoded chemical library based on chiral 4-amino-proline enables stereospecific isozyme-selective protein recognition. *Nat. Chem.* **15**, 1431–1443 (2023).
- Li, G. et al. Enantiopure Fell4L4 cages bind steroids stereoselectively. *Chem* **9**, 1549–1561 (2023).
- Han, X. N., Li, P. F., Han, Y. & Chen, C. F. Enantiomeric water-soluble octopus[3]arenes for highly enantioselective recognition of chiral ammonium salts in water. *Angew. Chem. Int. Ed.* **61**, e202202527 (2022).
- Hu, M. et al. Chiral recognition and enantiomer excess determination based on emission wavelength change of AIEgen rotor. *Nat. Commun.* **11**, 161 (2020).
- Hagelschuer, A., Padin, D., Daskova, V. & Feringa, B. L. Toward chiral recognition by design: uncovering the self-enantioresolving properties of chiral amine derivatives. *J. Am. Chem. Soc.* **147**, 18662–18673 (2025).
- Zhang, X., Yin, J. & Yoon, J. Recent advances in development of chiral fluorescent and colorimetric sensors. *Chem. Rev.* **114**, 4918–4959 (2014).
- Sheng, J., Pooler, D. R. S. & Feringa, B. L. Enlightening dynamic functions in molecular systems by intrinsically chiral light-driven molecular motors. *Chem. Soc. Rev.* **52**, 5875–5891 (2023).
- Peluso, P. & Chankvetadze, B. Recognition in the domain of molecular chirality: from noncovalent interactions to separation of enantiomers. *Chem. Rev.* **122**, 13235–13400 (2022).
- Zhang, Z. et al. Excited-state conformational/electronic responses of saddle-shaped N,N'-disubstituted-dihydrodibenzo[a,c]phenazines: wide-tuning emission from red to deep blue and white light combination. *J. Am. Chem. Soc.* **137**, 8509–8520 (2015).
- Zhang, Z., Sun, G., Chen, W., Su, J. & Tian, H. The endeavor of vibration-induced emission (VIE) for dynamic emissions. *Chem. Sci.* **11**, 7525–7537 (2020).
- Huang, Z., Jiang, T., Wang, J., Ma, X. & Tian, H. Real-time visual monitoring of kinetically controlled self-assembly. *Angew. Chem. Int. Ed.* **60**, 2855–2860 (2021).
- Zong, Z. et al. Dynamic timing control over multicolor molecular emission by temporal chemical locking. *Angew. Chem. Int. Ed.* **61**, e202116414 (2022).
- Zong, Z., Zhang, Q. & Qu, D.-H. A single-fluorophore multicolor molecular sensor that visually identifies organic anions including phosphates. *CCS Chem.* **6**, 774–782 (2024).
- Hu, W. et al. Real-time direct monitoring of chirality fixation and recognition at the single-molecule level. *J. Am. Chem. Soc.* **146**, 17765–17772 (2024).
- Ye, X. et al. Tuning organic crystal chirality by the molar masses of tailored polymeric additives. *Nat. Commun.* **12**, 6841 (2021).
- Ye, X., Wang, Z., Zhang, J. & Wan, X. Noncovalently functionalized commodity polymers as tailor-made additives for stereoselective crystallization. *Angew. Chem. Int. Ed.* **60**, 20243–20248 (2021).
- Liang, X. et al. Nitrogen-oxidized troger's base macrocyclic arenes: unprecedented enantioselective recognition in water. *Angew. Chem. Int. Ed.* **64**, e202416975 (2025).
- Maeda, K. et al. Helical springs as a color indicator for determining chirality and enantiomeric excess. *Sci. Adv.* **7**, eabg5381 (2021).
- Wang, S. M. et al. Chiral recognition of neutral guests by chiral naphthotubes with a bis-thiourea endo-functionalized cavity. *Nat. Commun.* **14**, 5645 (2023).
- Fu, R. et al. A chiral emissive conjugated corral for high-affinity and highly enantioselective recognition in water. *Angew. Chem. Int. Ed.* **62**, e202315990 (2023).
- Yang, Y., Liu, L. & Wei, Z. Chiral conjugated molecular assemblies interact with substances and light. *Acc. Mater. Res.* **5**, 329–346 (2024).
- Zhang, Y. D. et al. Review circularly polarized luminescence in chiral materials. *Matter* **5**, 837–875 (2022).
- He, Z., Huang, Z. & Ma, X. Lifetime-tunable circularly polarized luminescent system based on triplet-to-singlet Förster resonance energy transfer. *Sci. China Chem.* **67**, 2918–2922 (2024).

Acknowledgements

X.M. wishes to thank the National Key Research and Development Program of China (grant no. 2022YFB3203500), the National Natural Science Foundation of China (22125803, T2488302, 22020102006), Science and Technology Commission of Shanghai Municipality (grant No.24DX1400200), and the Fundamental Research Funds for the Central Universities. Z.-Z. H. wishes to thank the National Natural Science Foundation of China (22408106), China Postdoctoral Science Foundation (2024M760913), Shanghai Sailing Program (24YF2708500).

Author contributions

Z.-Z. H. and Y.H. contributed equally to this work. Z.-Z. H., Y.H., and X.M. designed the molecular structure and its synthesis route. Y.H., J.S., and Z.-Y.H. performed the synthesis of all molecules. T.J. performed the calculations. X.M. and H.T. conceived the project and supervised the experiment. Z.-Z.H. wrote the manuscript with the assistance from the other authors. All authors contributed to the analysis of the results and the writing of the manuscript.

Competing interests

The authors declare no competing interests.

Additional information

Supplementary information The online version contains supplementary material available at <https://doi.org/10.1038/s41467-025-63065-2>.

Correspondence and requests for materials should be addressed to Xiang Ma.

Peer review information *Nature Communications* thanks the anonymous reviewers for their contribution to the peer review of this work. A peer review file is available.

Reprints and permissions information is available at <http://www.nature.com/reprints>

Publisher's note Springer Nature remains neutral with regard to jurisdictional claims in published maps and institutional affiliations.

Open Access This article is licensed under a Creative Commons Attribution-NonCommercial-NoDerivatives 4.0 International License, which permits any non-commercial use, sharing, distribution and reproduction in any medium or format, as long as you give appropriate credit to the original author(s) and the source, provide a link to the Creative Commons licence, and indicate if you modified the licensed material. You do not have permission under this licence to share adapted material derived from this article or parts of it. The images or other third party material in this article are included in the article's Creative Commons licence, unless indicated otherwise in a credit line to the material. If material is not included in the article's Creative Commons licence and your intended use is not permitted by statutory regulation or exceeds the permitted use, you will need to obtain permission directly from the copyright holder. To view a copy of this licence, visit <http://creativecommons.org/licenses/by-nc-nd/4.0/>.

© The Author(s) 2025